JOURNAL OF MAGNETIC RESONANCE 81, 43–56 (1989)

A k-Space Analysis of Small-Tip-Angle Excitation

JOHN PAULY, DWIGHT NISHIMURA, AND ALBERT MACOVSKI

Information Systems Laboratory, Stanford University, Stanford, California 94305

Received December 7, 1987; revised April 11, 1988

We present here a method for analyzing selective excitation in terms of spatial frequency (**k**) space. Using this analysis we show how to design inherently refocused selective excitation pulses in one and two dimensions. The analysis is based on a small-tip model, but holds well for 90° tip angles. © 1989 Academic Press, Inc.

In this paper we present a new viewpoint for analyzing selective excitation for magnetic resonance imaging. The data acquisition and reconstruction phase of magnetic resonance imaging has very successfully been analyzed from the viewpoint of scanning spatial frequency, or **k**, space (*1–3*). Here we show that a similar approach may also be profitably applied to the excitation phase of magnetic resonance imaging. The excitation may be seen as scanning the applied RF energy across the same **k** space as is used for acquisition. This viewpoint is only strictly valid in the small-tip-angle regime. However, the results obtained continue to hold well for tip angles on the order of 90°.

We will present two new types of pulses that are suggested by the **k**-space approach that would not otherwise be evident. The first are slice-selective excitation pulses that are inherently refocused at the end of the excitation. No gradient refocusing lobes are needed. The second new type of pulses are those spatially selective in two dimensions. These pulses are useful for localized spectroscopy, for restricting the field of view in fast imaging, or for restricting the projection direction for projection imaging.

k-SPACE INTERPRETATION OF SMALL-TIP EXCITATION

The approach we are proposing for analyzing selective excitation is based on the well-known small-tip approximation (*4, 5*). Using this approximation an integral expression may be found for the transverse magnetization produced by a selective excitation pulse. This expression may be interpreted as scanning a path in a spatial frequency space, or **k** space.

Small-tip excitation. The Bloch equation in the rotating frame, neglecting T_1 and T_2, is

$$\begin{pmatrix} \dot{M}_x \\ \dot{M}_y \\ \dot{M}_z \end{pmatrix} = \gamma \begin{pmatrix} 0 & \mathbf{G}\cdot\mathbf{x} & -B_{1,y} \\ -\mathbf{G}\cdot\mathbf{x} & 0 & B_{1,x} \\ B_{1,y} & -B_{1,x} & 0 \end{pmatrix} \begin{pmatrix} M_x \\ M_y \\ M_z \end{pmatrix}. \qquad [1]$$

0022-2364/89 $3.00

G is the amplitude of the linear gradient, and B_1 is the amplitude of the applied RF field. Both are functions of time. The small-tip approximation assumes that the longitudinal magnetization M_z is approximately equal to its equilibrium value M_0,

$$M_z \approx M_0 = \text{constant}. \quad [2]$$

This is true provided the excitation pulse rotates the magnetization vector **M** only a small angle from the $+z$ axis. Under this assumption the first two components of Eq. [1] can be decoupled from the third. Define the transverse magnetization as

$$M_{xy} = M_x + iM_y, \quad [3]$$

and the applied RF field as

$$B_1 = B_{1,x} + iB_{1,y}. \quad [4]$$

Then the first two components of Eq. [1] can be written as the single complex differential equation

$$\dot{M}_{xy} = -i\gamma \mathbf{G}\cdot\mathbf{x} M_{xy} + i\gamma B_1 M_0. \quad [5]$$

If the system is initially in the state $(0, 0, M_0)$ this differential equation can be solved for the final magnetization at time T,

$$M_{xy}(\mathbf{x}) = i\gamma M_0 \int_0^T B_1(t) e^{-i\gamma \mathbf{x}\cdot\int_t^T \mathbf{G}(s)ds} dt. \quad [6]$$

This equation gives the transverse magnetization as a function of the applied RF and gradient fields, both of which are in general time-varying. We will be examining the implications of this equation in detail.

k-*space interpretation.* If we define a spatial frequency variable $\mathbf{k}(t)$ as

$$\mathbf{k}(t) = -\gamma \int_t^T \mathbf{G}(s)ds \quad [7]$$

then Eq. [6] may be rewritten

$$M_{xy}(\mathbf{x}) = i\gamma M_0 \int_0^T B_1(t) e^{i\mathbf{x}\cdot\mathbf{k}(t)} dt. \quad [8]$$

Note that in Eq. [7] the integration is from the time t to the time of the end of the excitation pulse. The function $\mathbf{k}(t)$ parametrically describes a path through spatial frequency space. We can write the exponential factor as an integral of a three-dimensional delta function

$$M_{xy}(\mathbf{x}) = i\gamma M_0 \int_0^T B_1(t) \int_{\mathbf{K}} {}^3\delta(\mathbf{k}(t) - \mathbf{k}) e^{i\mathbf{x}\cdot\mathbf{k}} d\mathbf{k}\, dt. \quad [9]$$

Interchanging the order of integration,

$$M_{xy}(\mathbf{x}) = i\gamma M_0 \int_{\mathbf{K}} \left\{ \int_0^T B_1(t)\, {}^3\delta(\mathbf{k}(t) - \mathbf{k}) dt \right\} e^{i\mathbf{x}\cdot\mathbf{k}} d\mathbf{k}. \quad [10]$$

The inner integral over time is the three-dimensional path which we will designate

$$p(\mathbf{k}) = \int_0^T B_1(t)^3\delta(\mathbf{k}(t) - \mathbf{k})dt. \quad [11]$$

This expression shows the explicit weighting of **k** space by the RF excitation $B_1(t)$. It also contains an implicit weighting due to the varying velocity with which **k** space is scanned. To make this weighting explicit we normalize the delta function by multiplying it by the derivative of its argument. To preserve the equation we must then divide by the same factor. The result is

$$p(\mathbf{k}) = \int_0^T \frac{B_1(t)}{|\gamma\mathbf{G}(t)|}\{^3\delta(\mathbf{k}(t) - \mathbf{k})\,|\dot{\mathbf{k}}(t)|\}dt, \quad [12]$$

where we have used the fact that $\dot{\mathbf{k}}(t) = \gamma\mathbf{G}(t)$ and assumed that $B_1(t)/|\gamma\mathbf{G}(t)|$ is finite. The term in braces is now a unit delta function. Equation [12] shows that the path scans **k** space weighted by $B_1(t)/|\gamma\mathbf{G}(t)|$. The expression for the transverse magnetization resulting from the selective excitation is then

$$M_{xy}(\mathbf{x}) = i\gamma M_0 \int_{\mathbf{K}} p(\mathbf{k})e^{i\mathbf{x}\cdot\mathbf{k}}d\mathbf{k}. \quad [13]$$

The resulting transverse magnetization is simply the Fourier transform of the weighted **k**-space trajectory.

A simpler and conceptually useful expression may be obtained for the case where the **k**-space trajectory does not cross itself. For this case we define a spatial weighting function

$$W(\mathbf{k}(t)) = \frac{B_1(t)}{|\gamma\mathbf{G}(t)|}. \quad [14]$$

$W(\mathbf{k})$ is left unspecified for **k** not on the $\mathbf{k}(t)$ trajectory. The idea is that $B_1(t)/|\gamma\mathbf{G}(t)|$ is a moving sample of a time-independent function $W(\mathbf{k})$. Later when we are concerned with designing selective excitation pulses this will become the Fourier transform of the desired localization. Substituting this expression back into Eq. [12] results in:

$$\begin{aligned} p(\mathbf{k}) &= \int_0^T W(\mathbf{k}(t))\{^3\delta(\mathbf{k}(t) - \mathbf{k})\,|\dot{\mathbf{k}}(t)|\}dt \\ &= W(\mathbf{k})\int_0^T \{^3\delta(\mathbf{k}(t) - \mathbf{k})\,|\dot{\mathbf{k}}(t)|\}dt. \end{aligned} \quad [15]$$

Here we have used the fact that $f(x)\delta(x - x_0) = f(x_0)\delta(x - x_0)$. In Eq. [15] the path $p(\mathbf{k})$ factors into two terms, the spatial weighting function $W(\mathbf{k})$ and a parametric description of the unit weight trajectory

$$S(\mathbf{k}) = \int_0^T \{^3\delta(\mathbf{k}(t) - \mathbf{k})\,|\dot{\mathbf{k}}(t)|\}dt. \quad [16]$$

$S(\mathbf{k})$ may be thought of as a sampling structure. It determines both the area and the density of the **k**-space representation. The expression for the transverse magnetization given in Eq. [13] may now be rewritten as

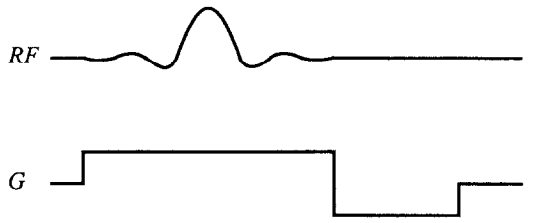

FIG. 1. Conventional slice-selective excitation. A constant slice-select gradient is applied while the RF waveform is played out. At the end of the RF the gradient is reversed to refocus the selected slice. The area of the refocusing lobe is one-half the area of the slice-select lobe in the small-tip-angle case.

$$M_{xy}(\mathbf{x}) = i\gamma M_0 \int_{\mathbf{K}} W(\mathbf{k})S(\mathbf{k})e^{i\mathbf{x}\cdot\mathbf{k}}d\mathbf{k}. \qquad [17]$$

The transverse magnetization is the Fourier transform of a spatial frequency weighting function $W(\mathbf{k})$ multiplied by a spatial frequency sampling function $S(\mathbf{k})$. We will return to this expression when we consider the design of selective excitation pulses.

APPLICATIONS OF THE k-SPACE INTERPRETATION

The **k**-space interpretation of small-tip excitation immediately suggests several new pulse sequences, two of which will be presented here. Before proceeding with these we will illustrate the concepts involved by applying the new formalism to a familiar example.

Conventional slice-selective excitation. The conventional slice-selective excitation pulse sequence is shown in Fig. 1. A constant gradient is applied as a sinc RF waveform is played out. This produces an approximately rectangular slice profile. After the RF waveform has ended the gradient is reversed to refocus the selected slice. In the small-tip case the area under the refocusing lobe is one-half the area under the slice-select lobe.

The **k**-space interpretation is illustrated in Fig. 2. **k**-space is scanned linearly as the RF field is applied. Note that in Eq. [7] the location in **k** space at a time t is the integral of the *remaining* gradient waveform. Hence the origin in **k** space is reached when the remaining gradient integrates to 0. This occurs halfway through the slice-select gradient lobe, and halfway through the RF excitation. The RF weighting is then

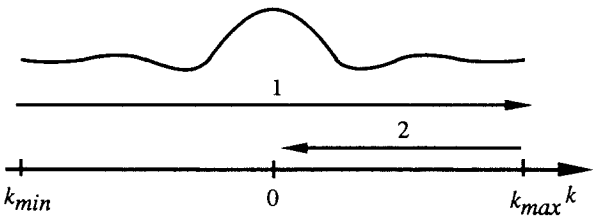

FIG. 2. **k**-space interpretation of the pulse sequence in Fig. 1. (1) The slice-select gradient scans **k** space linearly while the RF waveform is applied. (2) The refocusing lobe shifts the origin of **k** space back to the middle of the symmetric RF weighting.

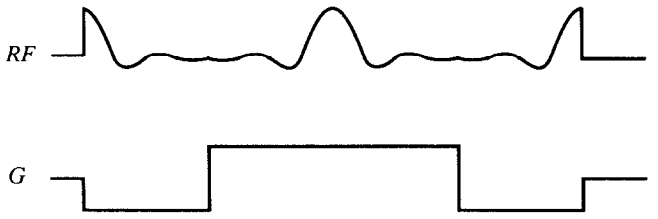

FIG. 3. An inherently refocused slice-selective excitation pulse sequence. This is similar to the pulse sequence in Fig. 1. It differs in that there is an additional negative gradient lobe before the slice-select gradient, and in that RF is applied the entire time the gradients are on. The RF polarity is the same for either gradient polarity.

centered in **k** space and is symmetric about the origin. The slice profile, which is the Fourier transform of this RF weighting, is in phase. During the refocusing lobe no RF is applied. Its purpose is simply to shift the **k**-space origin back to the middle of the RF excitation.

Inherently refocused pulses. This description of the conventional slice-selective excitation suggests several generalizations. First, RF can be applied throughout the excitation pulse sequence provided the desired weighting of **k** space is still achieved. Second, any RF and gradient waveform pair that ends at the middle of a symmetric weighting of **k** space will automatically be refocused.

A simple example of this is the pulse sequence shown in Fig. 3. Again, **k** space is weighted by a sinc as it was in the conventional case. The **k**-space interpretation of this pulse sequence is shown in Fig. 4. The first gradient lobe scans **k** space from the origin in the negative direction to $k_{\min}$. During this lobe half of the sinc waveform is applied, starting at zero frequency. The second gradient lobe scans **k** space from $k_{\min}$ to $k_{\max}$ while the whole sinc waveform is played out on the RF. The last gradient lobe scans **k** space from $k_{\max}$ back to the origin while the last half of the sinc waveform is applied, ending at zero frequency. The result is that **k** space is symmetrically covered twice by the RF excitation. Since the **k**-space trajectory ends at the middle of this symmetric weighting the selected slice is in-phase.

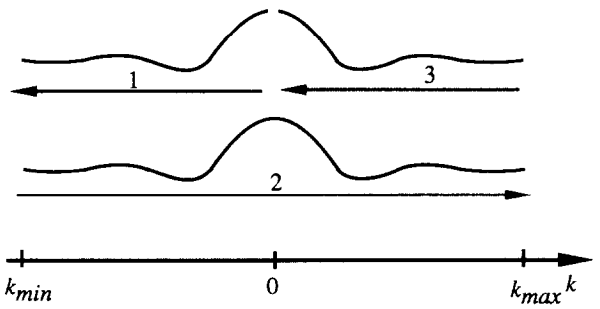

FIG. 4. **k**-space interpretation of the pulse sequence in Fig. 3. (1) During the first gradient lobe the negative part of **k**-space is weighted by half of the sinc waveform. (2) During the second gradient lobe the whole **k**-space interval is weighted by the sinc waveform. (3) The third lobe returns to the origin while the other half of the sinc is applied. The result is that **k** space is covered twice by the RF excitation.

This pulse sequence is very similar to the conventional slice-selective excitation pulse sequence discussed in the previous subsection. If the RF is turned off during the first and last lobes, the two are exactly the same. However, by scanning **k** space twice the RF amplitude required is halved, the peak RF power is quartered, and the total RF power is halved. One disadvantage of this pulse is some sensitivity to chemical shift.

Slice profiles for this pulse are given in Figs. 5 and 6. These were obtained by numerical integration of the Bloch equation. Figure 5 shows the slice profile for a 30° tip angle. This is approximately the limit of the small-tip-angle regime. The transverse magnetization is almost entirely in the imaginary component, M_y. This indicates the slice is very well refocused. Figure 6 shows the slice profile for a 90° tip angle. This is well beyond the small-tip-angle regime. However, the slice profile is still reasonably well focused. Improved refocusing could be obtained with minor modifications of the gradient amplitudes. Even though this pulse sequence was designed using small-tip-angle arguments it still works well for tip angles on the order of 90°.

This approach also has the practical benefit of indicating how to utilize nonconstant slice-select gradients. The abrupt transitions required for the gradient waveform in Fig. 3 are difficult to produce practically. This is not a fundamental problem, since the critical quantity is the weighting of **k** space. This is the ratio $B_1(t)/|\gamma \mathbf{G}(t)|$. Any gradient waveform can be used provided it covers the necessary part of **k** space, and provided the RF waveform is compensated to produce the desired weighting. This is a special case of the more general variable-rate selective excitation principle VERSE described in (*6*).

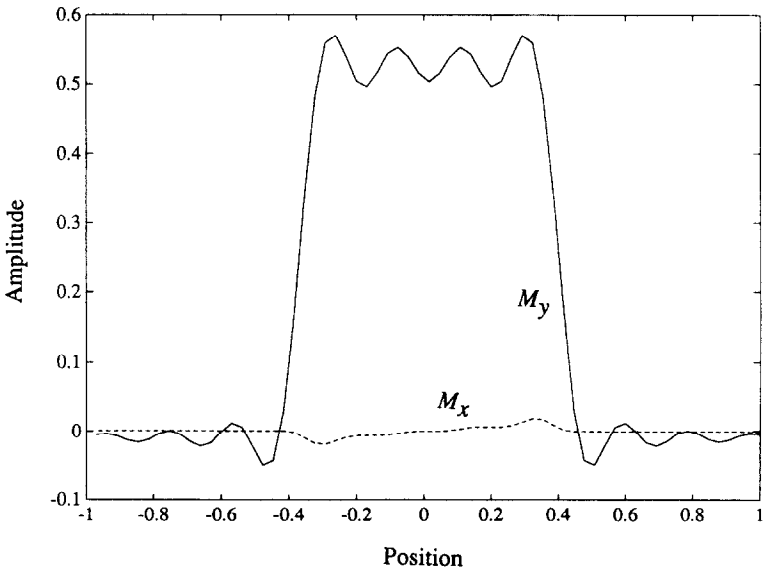

FIG. 5. Slice profile resulting from the pulse sequence in Fig. 3. The tip angle here is 30° which is approximately the limit of the small-tip approximation. The M_x component of the transverse magnetization is small, indicating the slice is well refocused.

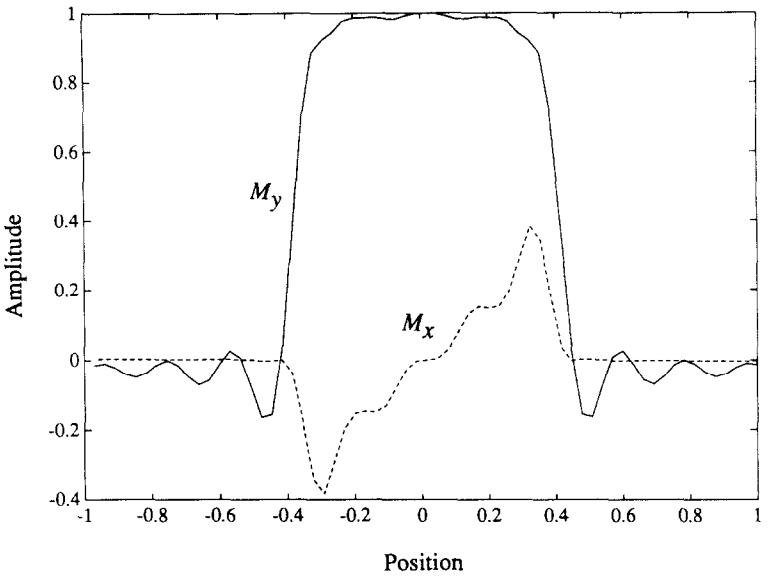

FIG. 6. Slice profile for the same pulse sequence as Fig. 5, but with the excitation scaled to produce a tip angle of 90°. This is well beyond the small-tip-angle regime for which the pulse was designed. Nonetheless, the pulse is still reasonably well refocused across the slice. This can be improved by minor adjustments to the gradient amplitudes.

Two-dimensional selective excitation. In the previous two subsections we have been talking about the familiar problem of selectively exciting a slice. In this subsection we describe how this can be extended to two dimensions. An approach has recently been presented for achieving two-dimensional spatial localization for spectroscopy (*7–9*), by design of selective two-dimensional 180° pulses. Our approach here differs in two respects. First we are concerned with designing inherently refocused two-dimensional selective excitation pulses. Second, we show here an analytic approach for designing and analyzing the required RF and gradient waveforms.

The problem of a spatially localizing excitation in two dimensions exactly parallels the problem of reconstructing an image from data taken with time-varying gradients (*1, 2, 10–15*). In both cases the goal is to cover some region of spatial frequency space by a gradient-controlled trajectory. And, in both cases the resolution element or selective volume is the Fourier transform of this weighted trajectory.

Almost any of the methods that have been proposed for producing an MR image from one FID can also be used to produce two-dimensional spatially localized excitation. These include echo planar and its variations (*10, 11*), constant-angular-rate spirals (*2, 14*), constant-velocity spirals (*15*), and square spirals (*15*). The difference is that instead of acquiring data as the gradient field is applied, an RF field is applied to achieve the desired spatial frequency weighting. Note that as in the previous subsection, if **k** space is weighted symmetrically and the **k**-space trajectory ends at the origin, then the selected volume is automatically refocused.

The design of a two-dimensional selective excitation starts by choosing a spatial frequency weighting function $D(\mathbf{k})$ whose Fourier transform is the desired localiza-

tion. Referring back to Eq. [17] we see that we want to find a spatial frequency weighting function $W(\mathbf{k})$ and spatial frequency sampling function $S(\mathbf{k})$ such that $W(\mathbf{k})S(\mathbf{k})$ is a good approximation to $D(\mathbf{k})$. The choice of $S(\mathbf{k})$ corresponds to choosing a **k**-space scanning trajectory, like the echo-planar or the square-spiral trajectories mentioned above. The requirements for the trajectory are exactly the same for excitation as they are for imaging. The trajectory should uniformly cover the part of **k** space where $D(\mathbf{k})$ has significant energy, and it should cover this region with sufficient density to limit aliasing. Given that $S(\mathbf{k})$ fulfills these requirements we can let the weighting function be the desired spatial frequency weighting $W(\mathbf{k}) = D(\mathbf{k})$.

As an example we will describe the design of a circularly symmetric Gaussian localization excitation. The desired spatial frequency weighting $D(\mathbf{k})$ is then also a circularly symmetric Gaussian function.

For a **k**-space trajectory we choose a constant-angular-rate spiral. This is illustrated in Fig. 7. Since we want to end up at the origin at the end of the pulse we start out at the edge of the spiral end and come in. This assures that the slice will be refocused automatically. We could also start at the middle and spiral out, but then we would need a refocusing lobe at the end. This **k**-space trajectory can be written as

$$k_x(t) = A\left(1 - \frac{t}{T}\right)\cos\frac{2\pi nt}{T}$$

$$k_y(t) = A\left(1 - \frac{t}{T}\right)\sin\frac{2\pi nt}{T}, \qquad [18]$$

where the spiral has n cycles in a time T. In Fig. 7 $n = 8$. In the radial dimension **k** space is covered discretely. This will produce radial sidelobes, exactly analogous to aliasing due to a limited sampling rate. The number of cycles n determines how far

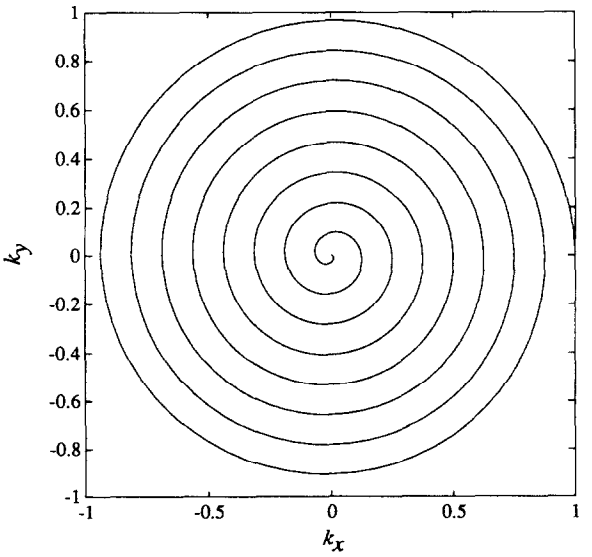

FIG. 7. **k**-space trajectory for a spiral two-dimensional selective excitation. The spiral is started at the outer edge and ended at the middle so that the selected volume will be inherently refocused. No refocusing gradient lobes are required. This spiral corresponds to Eq. [18] with $n = 8$.

out the first aliasing sidelobe will be. The factor A in Eq. [18] determines the size of the spiral in spatial frequency. The gradient waveforms that produce this $\mathbf{k}$ trajectory are $\mathbf{G}(t) = (1/\gamma)\dot{\mathbf{k}}(t)$,

$$G_x(t) = -\frac{A}{\gamma T}\left[2\pi n\left(1 - \frac{t}{T}\right)\sin\frac{2\pi nt}{T} + \cos\frac{2\pi nt}{T}\right]$$

$$G_y(t) = \frac{A}{\gamma T}\left[2\pi n\left(1 - \frac{t}{T}\right)\cos\frac{2\pi nt}{T} - \sin\frac{2\pi nt}{T}\right]. \qquad [19]$$

These are plotted in Fig. 8.

The desired spatial frequency weighting is a circularly symmetric Gaussian function, which can be written as

$$D(\mathbf{k}) = \alpha e^{-\beta^2(k_x^2+k_y^2)/A^2}. \qquad [20]$$

The quantity α scales the tip angle, while β determines the spatial resolution of the selective volume. Given that the spiral adequately samples $\mathbf{k}$ space, we let $W(\mathbf{k}) = D(\mathbf{k})$. Then using Eq. [14] we can calculate the required RF waveform,

$$\begin{aligned} B_1(t) &= W(\mathbf{k}(t))\,|\gamma\mathbf{G}(t)| \\ &= \alpha e^{-\beta^2(k_x^2(t)+k_y^2(t))/A^2}\gamma\frac{A}{T}\sqrt{\left[2\pi n\left(1-\frac{t}{T}\right)\right]^2 + 1} \\ &= \gamma\alpha\frac{A}{T}e^{-\beta^2(1-t/T)^2}\sqrt{\left[2\pi n\left(1-\frac{t}{T}\right)\right]^2 + 1}. \end{aligned} \qquad [21]$$

This is plotted in Fig. 9 for the case where $\beta = 2$.

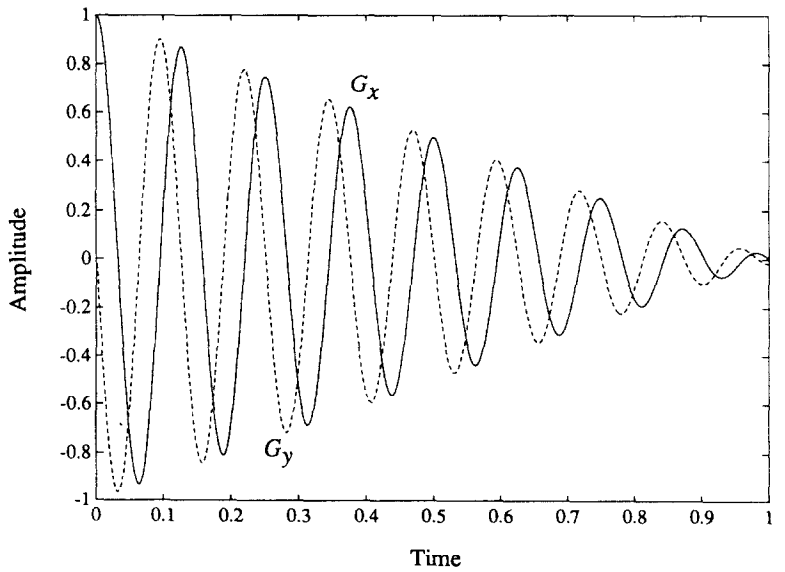

FIG. 8. Gradient waveforms that will produce the k-space trajectory shown in Fig. 7. These are given mathematically by Eq. [19] with $n = 8$.

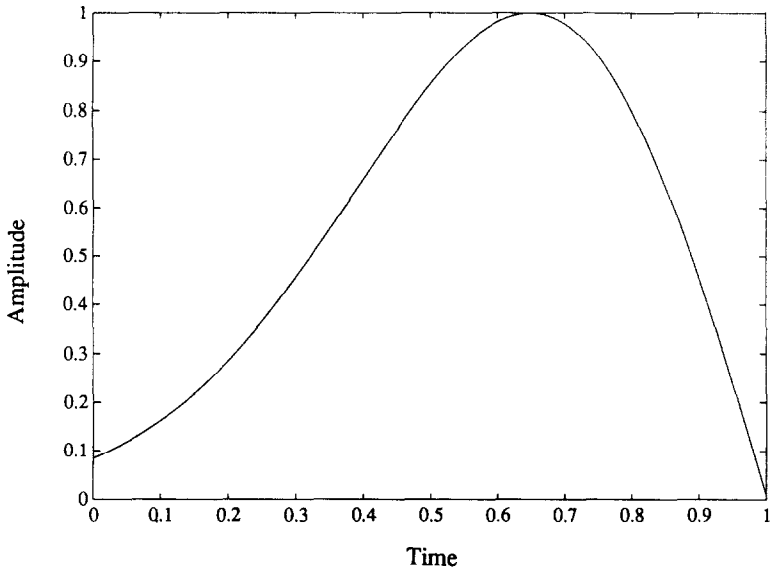

FIG. 9. RF waveform that will produce a cylindrical Gaussian weighting of k space when applied with the gradient waveforms shown in Fig. 8. This waveform is given by Eq. [21] with $\beta = 2$.

The selective volume that results from this gradient and RF combination is plotted in Figs. 10 and 11. Figure 10 is a surface plot of the real and imaginary part of M_{xy} resulting from a 30° tip angle. Note that there is virtually no real component. The resulting magnetization is all along M_y. This means the volume is very well refocused. Also note that the sidelobes are very low. Figure 11 is a surface plot of the excitation scaled to a 90° tip angle. This is well beyond the small-tip-angle regime. The slice is again very well focused, and again the sidelobes are very low. This excitation pulse performs very well for tip angles on the order of 90°.

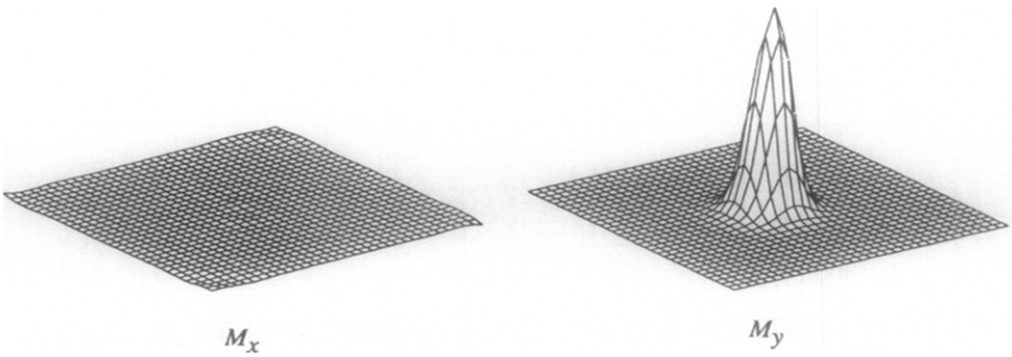

FIG. 10. Surface plots of the selective volume produced gradient waveform in Fig. 8 with the RF waveform in Fig. 9. The RF is scaled to produce a tip angle of 30°. The left plot is M_x, and the right plot is M_y. Note that virtually all of the transverse magnetization is in M_y, meaning the selected volume is very well refocused. Also the sidelobes are very low.

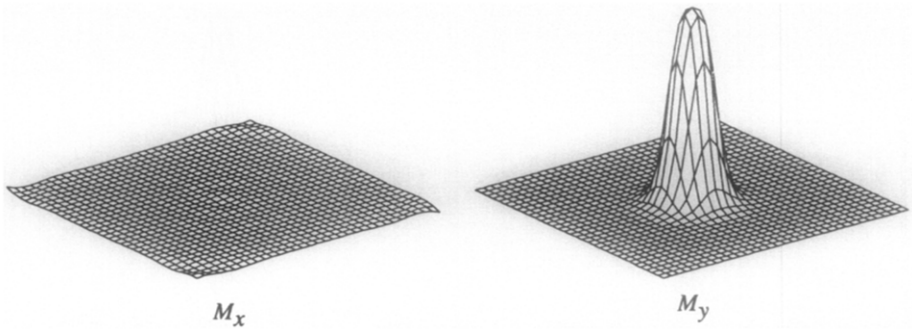

FIG. 11. Surface plots for the same RF and gradient waveforms as in Fig. 10, but with the RF scaled to a tip angle of 90°. This is well beyond the small-tip-angle regime. In spite of this the slice profile is very good. The phase of the transverse magnetization is very well focused, and the sidelobes are low.

The selective volume can also be shifted to other spatial positions. To see this consider the effect of the following RF waveform:

$$B_1'(t) = B_1(t)e^{-i\mathbf{x}_0\cdot\mathbf{k}(t)}. \qquad [22]$$

Substituting this into Eq. [8],

$$\begin{aligned} M_{xy}(\mathbf{x}) &= \gamma M_0 \int_0^T B_1(t)e^{-i\mathbf{x}_0\cdot\mathbf{k}(t)}e^{i\mathbf{x}\cdot\mathbf{k}(t)}dt \\ &= \gamma \mathbf{M}_0 \int_0^T B_1(t)e^{i(\mathbf{x}-\mathbf{x}_0)\cdot\mathbf{k}(t)}dt. \end{aligned} \qquad [23]$$

The excitation has been shifted spatially to the position $\mathbf{x}_0$.

A concern with these two-dimensional selective excitation pulses is spectral sensitivity. The **k**-space analysis can easily be extended to include an additional spectral axis. This is beyond the scope of the present paper. Here we will simply note the nature of off-resonance effects. First, the duration of these pulses will result in some spectral selectivity. Second, there is a phase shift proportional to offset frequency. This can be refocused using a 180° pulse, just as a constant slice-selective excitation pulse is refocused by reversing the slice-select gradient. Third, the spatial selectivity of the pulse degrades with increasing offset frequency. This is a result of the particular **k**-space trajectory chosen.

As an example we calculated the selective volume corresponding to Fig. 11 with a half cycle off-resonance shift over the duration of the pulse. This represents approximately 1 ppm shift for an 8 ms pulse at 1.5 T. The result is shown in Fig. 12. We have assumed refocusing with a 180° pulse followed by a delay of 0.45 times the pulse length. The M_y component is relatively unchanged. The principal effect is the presence of an M_x component. This represents both some loss in resolution and imperfect spatial phase coherence. These effects can be reduced by reducing the duration of the pulse, or by using a different **k**-space trajectory. In particular an echo-planar-type excitation pulse will suffer almost no resolution degradation, although spectral shift will spatially shift the resolution volume in the slow gradient direction.

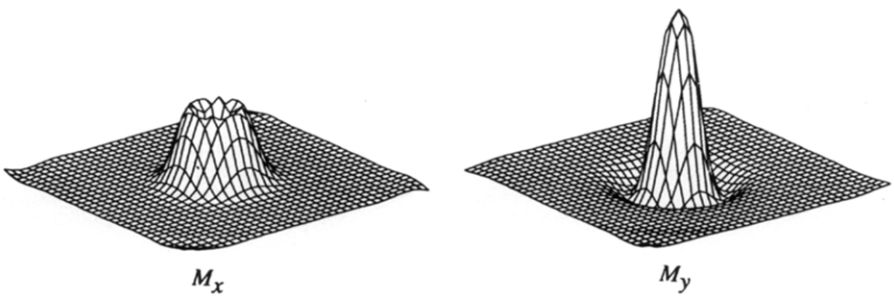

FIG. 12. Selective volume resulting from the same excitation as in Fig. 11, but with a half cycle off-resonance shift over the duration of the pulse. This corresponds to a 1 ppm shift for an 8 ms excitation pulse at 1.5 T. We have assumed the volume has been refocused with a 180° pulse. The M_y component is relatively unaffected from Fig. 11. The principal effect is a nonzero M_x representing some loss in resolution and imperfect phase coherence across the volume.

EXPERIMENTAL RESULTS

The selective excitation pulses described in the previous section are interesting from a theoretical viewpoint. To show that such pulses are useful practically, the two-dimensional selective excitation pulse was implemented on a 1.5 T General Electric Signa system. The system is stock in all relevant aspects and does not have shielded gradient coils.

The pulse sequence is illustrated in Fig. 13. The two-dimensional selective excitation is applied to the x and y axes. This will excite a cylinder along the z axis. A slice

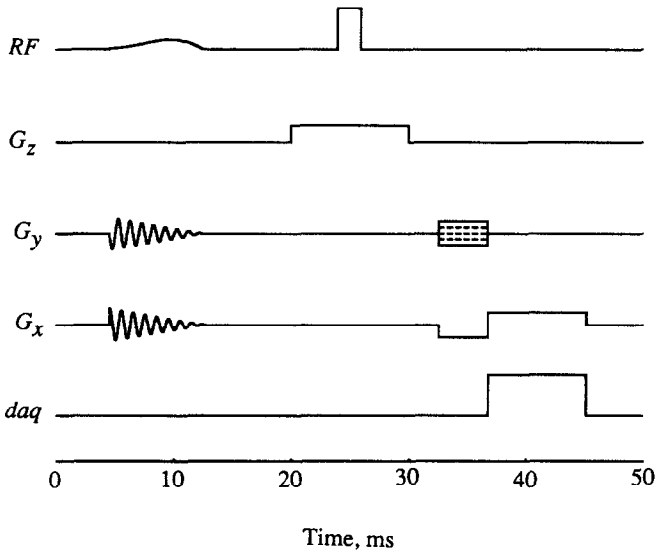

FIG. 13. Pulse sequence used to demonstrate the two-dimensional selective excitation pulse. The two-dimensional pulse is applied along the x and y axes exciting a cylinder along the z axis. A selective 180° forms a spin echo of a slice of this cylinder. The resulting disk is then imaged with a conventional spin-warp pulse sequence.

of this cylinder is selected using a slice-selective 180° refocusing pulse. The resulting disk is then imaged using a conventional spin-warp imaging sequence.

An image of the localized volume is shown in Fig. 14. The phantom is a large volume of water doped with $CuSO_4$ to a T_2 of 200 ms. Also shown is a profile along a diameter of the selected volume. The duration of the two-dimensional selective excitation was 8 ms, and the maximum gradient amplitude was 0.6 G/cm. The RF was scaled to produce a 90° excitation. The field of view is 24 cm, and the width of the selected volume is on the order of 3 cm. The first aliasing side lobe due to radial sampling is outside of the phantom, which is 28 cm in diameter.

CONCLUSION

In this paper we have proposed a new viewpoint for analyzing selective excitation. Selective excitation may be considered to be a weighted scan through a spatial frequency space. The slice profile is simply the Fourier transform of this weighted trajectory. Although only strictly valid for small-tip-angle excitation, the results for the cases considered here hold well at tip angles of 90°. From this viewpoint it is possible to propose new types of pulses that would not be readily apparent otherwise. Two that were presented here are excitation pulses that are inherently refocused, and excitation pulses that are spatially selective in two dimensions. This type of analysis can also be extended to other nonspatial axes such as chemical shift and velocity. This will be the subject of a subsequent paper.

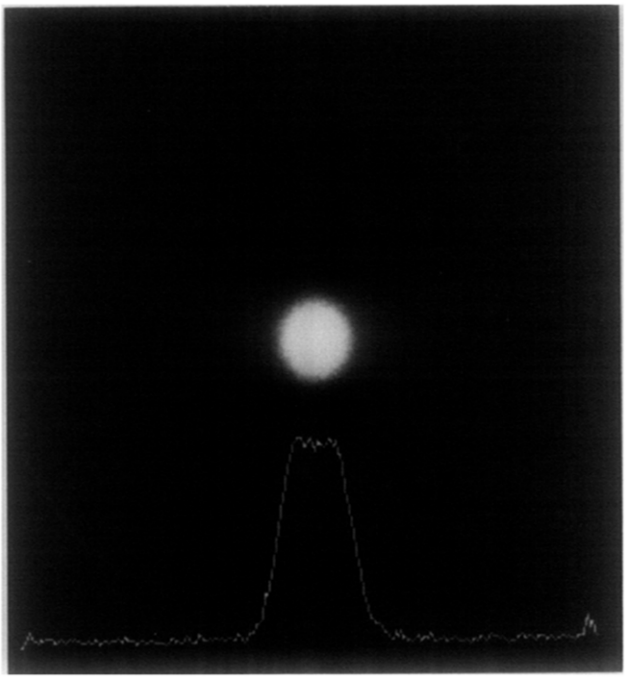

FIG. 14. Image of the selected volume resulting from the pulse sequence shown in Fig. 13. Also shown is a profile along a diameter of the selected volume. The two-dimensional selective excitation had a duration of 8 ms, and a peak gradient amplitude of 0.6 G/cm. The RF was scaled to produce a 90° tip angle. The field of view is 24 cm, and the diameter of the selected volume is approximately 3 cm.

ACKNOWLEDGMENTS

The authors gratefully acknowledge the support of the General Electric Medical Systems Division. This work was also supported by the National Institutes of Health Contract HV-38045 and Grant HL-34962.

Note added in proof. Dr. Norbert Pelc has recently pointed out Ref. (*16*) to the authors. It contains several other interesting **k**-space trajectories for magnetic resonance imaging data aquisition, as well as the design of a slice-selective excitation pulse using **k**-space ideas.

REFERENCES

1. D. B. TWIEG, *Med. Phys.* **10,** 610 (1983).
2. S. LJUNGGREN, *J. Magn. Reson.* **54,** 338 (1983).
3. T. R. BROWN, B. M. KINCAID, AND K. UGURBIL, *Proc. Natl. Acad. Sci. USA* **79,** 3523 (1982).
4. D. I. HOULT, *J. Magn. Reson.* **35,** 66 (1979).
5. W. S. HINSHAW AND A. H. LENT, *Proc. IEEE* **71**(3), 338 (1983).
6. S. CONOLLY, D. NISHIMURA, A. MACOVSKI, AND G. GLOVER, *J. Magn. Reson.* **78,** 440 (1988).
7. P. A. BOTTOMLEY, C. J. HARDY, AND W. M. LEUE, *In* "Proceedings Sixth SMRM," p. 133 (1987).
8. C. J. HARDY, M. O'DONNELL, P. A. BOTTOMLEY, AND P. ROEMER, *In* "Proceedings Sixth SMRM," p. 479 (1987).
9. P. A. BOTTOMLEY AND C. J. HARDY, *J. Magn. Reson.* **74,** 550 (1987).
10. P. MANSFIELD, *J. Phys. C* **10,** L55 (1977).
11. P. MANSFIELD AND P. G. MORRIS, "Advances in Magnetic Resonance: NMR Imaging in Biomedicine," Suppl. No. 2, Academic Press, New York, 1982.
12. A. MACOVSKI, *Magn. Reson. Med.* **2,** 29 (1985).
13. I. SHENBERG AND A. MACOVSKI, *IEEE Trans. Med. Imaging* **MI-5**(3), 121 (1986).
14. C. B. AHN, J. H. KIM, AND Z. H. CHO, *IEEE Trans. Med. Imaging* **MI-5**(1), 2 (1986).
15. A. MACOVSKI AND C. MEYER, *In* "Proceedings, Fifth SMRM, WIP," p. 156 (1986).
16. R. S. LIKES, U.S. Patent 4,307,343 (1981).